

Electromotive force in the Blandford-Znajek process

Kenji Toma^{1,2,3*} and Fumio Takahara³

¹*Astronomical Institute, Tohoku University, Sendai 980-8578, Japan*

²*Frontier Research Institute for Interdisciplinary Sciences, Tohoku University, Sendai 980-8578, Japan*

³*Department of Earth and Space Science, Graduate School of Science, Osaka University, Toyonaka 560-0043, Japan*

ABSTRACT

One of the mechanisms widely considered for driving relativistic jets in active galactic nuclei, galactic microquasars, and gamma-ray bursts is the electromagnetic extraction of the rotational energy of a central black hole, i.e., the Blandford-Znajek process, although the origin of the electromotive force in this process is still under debate. We study this process as the steady unipolar induction in the Kerr black hole magnetosphere filled with a collisionless plasma screening the electric field (the \mathbf{D} field) along the magnetic field (the \mathbf{B} field), i.e., $\mathbf{D} \cdot \mathbf{B} = 0$. We extend the formulations and arguments made by Komissarov, and generally show that the origin of the electromotive force is ascribed to the ergosphere. It is explicitly shown that open magnetic field lines penetrating the ergosphere have a region where the \mathbf{D} field is stronger than the \mathbf{B} field in the ergosphere, and it keeps driving the poloidal currents and generating the electromotive force and the outward Poynting flux. The range of the possible value of the so-called angular velocity of the magnetic field line Ω_F is deduced for the field lines threading the equatorial plane in the ergosphere. We briefly discuss the relation between our conclusion and the ideal magnetohydrodynamic condition.

Key words: black hole physics – magnetic fields – relativistic processes.

1 INTRODUCTION

Collimated outflows, or jets, with relativistic speeds are observed in active galactic nuclei and galactic microquasars, and are presumably driven in gamma-ray bursts. Possible mechanisms for driving relativistic jets include the electromagnetic extraction of the rotational energy of a central black hole (BH) (Blandford & Znajek 1977), the electromagnetic extraction of the rotational energy of an accretion flow around a BH (Lovelace 1976), and the thermal gas ejection from an accretion flow (e.g., Paczynski 1990; Asano & Takahara 2009; Becker et al. 2011; Toma & Takahara 2012).

The electromagnetic extraction of the rotational energy of the accretion flow is the same mechanism as pulsar winds. Goldreich & Julian (1969) showed that when the poloidal magnetic field is penetrating a rotating conductive star, the steady force-free magnetosphere can be established outside the star, where the poloidal electric fields are maintained by the charge distribution and the poloidal currents flow (i.e., the unipolar induction process). As a result, outward electromagnetic energy and angular momentum fluxes continue to be generated. The origin of the electromotive force (and the fluxes) is the matter-dominated rotating star, while the plasma outside the star only supports the electromagnetic

field, playing a passive role for keeping the electric potential differences in the whole system.

As for the energy extraction of the BH itself, Blandford & Znajek (1977) first showed a mathematical solution for the electromagnetic energy and angular momentum fluxes extracted from the BH with the force-free approximation in the slow rotation limit of the BH, in a similar mechanism to the Goldreich-Julian model. It has been frequently argued that this electromagnetic process may be the only viable process to extract the rotational energy from a BH (e.g., Bejger et al. 2012; Bardeen et al. 1972; Penrose 1969). However, the origin of the electromotive force in this process is still being debated. There is no matter-dominated region in which the poloidal magnetic field is anchored, and all the matter in the BH magnetosphere only plays a passive role. Then it is not a simple question what determines the electric potential difference (or the so-called angular velocity of the magnetic field line Ω_F) and drives the poloidal currents. The literature on the origin of the electromotive force focuses on either the event horizon (Thorne et al. 1986), the wind separation surface (Takahashi et al. 1990; Beskin & Kusnetsova 2000; Levinson 2006; Beskin 2010; Okamoto 2012), or the ergosphere (Komissarov 2004a, 2009) (see also Menon & Dermer 2005, 2011; Contopoulos et al. 2013), although the first one is unlikely because the event horizon is causally disconnected

* E-mail: toma@astr.tohoku.ac.jp

from the BH exterior (Punsly & Coroniti 1989; Punsly 2008; Beskin & Kusnetsova 2000).

The above literature mainly uses the analytical methods, while the numerical simulations based on the ideal magnetohydrodynamic (MHD) approximation have been actively performed to investigate the nature of the BH magnetosphere (and even its interaction with the accretion flow) (e.g., Koide et al. 2002; Komissarov 2005; McKinney 2006; Komissarov & Barkov 2009; Tchekhovskoy et al. 2011). Based on the simulation results, it was proposed that the unavoidable rotation of the fluids in the ergosphere generates MHD waves propagating outwards, and its feedback causes the fluids to have negative hydrodynamic energy as measured at infinity. They plunge into the BH, decreasing its rotational energy (Koide et al. 2002). However, the long-term simulations have demonstrated that no regions of negative hydrodynamic energy are seen in the steady state (Komissarov 2005), and thus more studies are required to understand the real mechanism of the extraction of the BH rotational energy (Komissarov 2009). Furthermore, it has not been discussed what determines the value of Ω_F and drives the poloidal currents by utilizing the MHD simulation results, as far as we are aware.

Since the Blandford-Znajek process is purely electromagnetic, the force-free simulations appear more suitable than the MHD simulations for investigating the nature of its mechanism (without including the complicated interaction of the BH magnetosphere with the accretion flow). Komissarov (2004a) clearly shows that when the BH exterior is vacuum, the electric field (the \mathbf{D} field) can be stronger than the magnetic field (the \mathbf{B} field) in the ergosphere, and performed the resistive force-free numerical simulations of the plasma-filled BH magnetosphere, demonstrating that such a strong electric field drives the poloidal currents. A similar conclusion was drawn from simulation results of the force-free electromagnetic field on highly compact regular space-times (i.e., with no event horizon) with an ergosphere (Ruiz et al. 2012). However, it has not been evident why the electric field is maintained to be strong in the plasma-filled BH magnetosphere and how the steady state with $\Omega_F > 0$ and non-zero poloidal currents is realized. A related question is whether the steady state with $\Omega_F = 0$ and/or zero poloidal currents is possible or not.

In this paper, we extend the argument of Komissarov (2004a), providing more general insights. We consider the steady, axisymmetric Kerr BH magnetosphere filled with a collisionless plasma satisfying $\mathbf{D} \cdot \mathbf{B} = 0$, and show in a fully analytical way that for open magnetic field lines threading the ergosphere, the state with $\Omega_F > 0$ and non-zero poloidal currents is forced to be maintained, i.e., the outward Poynting flux inevitably keeps being generated. The origin of the electromotive force is ascribed to the ergosphere. We show a self-consistent electromagnetic structure along an open field line threading the equatorial plane in the ergosphere, and deduce the range of the possible value of Ω_F for such field lines.¹ Our assumptions for the magnetospheric plasma are stated in Section 4.1, which do not rely on a specific Ohm's

law as done in Komissarov (2004a), the force-free condition ($F_{\mu\nu}I^\nu = 0$), nor the ideal MHD condition ($F_{\mu\nu}u^\nu = 0$).

This paper is organized as follows. We first review the Goldreich-Julian model of pulsar winds in Section 2 and the convenient formulation of the electrodynamics in Kerr space-time in Section 3. We then study the plasma-filled BH magnetosphere, discussing its general properties (Section 4) and the origin of the electromotive force (Section 5). Section 6 is devoted to summary and discussion.

2 UNIPOLAR INDUCTION OF PULSARS

We review the unipolar induction mechanism of pulsars, first discussed by Goldreich & Julian (1969), *which is quite helpful for understanding the unipolar induction of rotating BHs*. In particular, it is instructive that the electric field outside the star is stronger in the plasma-filled case than that in the vacuum case (equations 6 and 7) and that the star drives the poloidal currents inside itself in the direction of $-\mathbf{E}$, which generates the Poynting flux (equation 10). We will refer to these points in Section 5.1 and in Section 5.3, respectively.

2.1 Electric Potential Differences

Let us consider a uniformly magnetized, rotating star with angular velocity Ω_s . Our assumptions are as follows: (1) The rotation vector is parallel to the magnetic dipole moment, so that the system is steady and axisymmetric. (2) At and inside the stellar surface, the matter is highly conductive, and its rotational energy dominates the total energy. (3) The region outside the star is filled with plasma. The plasma is dilute and collisionless, but its number density is high enough to screen the electric field along the magnetic field lines, i.e., $\mathbf{E} \cdot \mathbf{B} = 0$ is satisfied. The energy density of the particles is much smaller than that of the electromagnetic field. The magnetic field is so strong that the gravitational force of the central star is negligible compared with the Lorentz force. In this section, we adopt the units of $c = 1$.

First of all, at and inside the stellar surface, the high conductivity implies

$$\mathbf{E} = -\mathbf{V} \times \mathbf{B} = -\varpi\Omega_s\mathbf{e}_\varphi \times \mathbf{B}, \quad (1)$$

where \mathbf{V} is the fluid velocity, and we have adopted the cylindrical coordinate system (ϖ, φ, z) . This electric field is produced by the non-zero charge density $\rho = (1/4\pi)\nabla \cdot \mathbf{E}$.

The electromagnetic field structure in the region outside the star, i.e., magnetosphere, is described as follows. In the axisymmetric configuration, the poloidal magnetic field can be written as

$$\mathbf{B}_p = \frac{1}{\varpi}\nabla\Psi \times \mathbf{e}_\varphi, \quad (2)$$

where $\Psi(\varpi, z)$ is called the flux function, representing the toroidal component of the vector potential times ϖ , or the magnetic flux threading through a circle of ϖ for a given z . The above equation leads to $\mathbf{B} \cdot \nabla\Psi = 0$, which means that $\Psi(\varpi, z)$ is constant along each magnetic field line. As for the electric field, Faraday's law in the steady state gives

way to the pulsar wind case. Such a situation is different from that we consider in this paper.

¹ Punsly & Coroniti (1990) proposed a MHD model for the unipolar induction for the poloidal magnetic field threading the equatorial plane in the ergosphere, but they argue that the potential difference is determined by the particle inertia in a similar

$\nabla \times \mathbf{E} = 0$. The axisymmetric condition implies $E_\varphi = 0$. This equation and $\mathbf{E} \cdot \mathbf{B} = 0$ mean that the electric field can be written as

$$\mathbf{E} = -\varpi \Omega_F \mathbf{e}_\varphi \times \mathbf{B}, \quad (3)$$

where Ω_F is a function of (ϖ, z) . Substituting this equation into $\nabla \times \mathbf{E} = 0$ and using $\nabla \cdot \mathbf{B} = 0$, one obtains

$$\mathbf{B} \cdot \nabla \Omega_F = 0. \quad (4)$$

This means that Ω_F is constant along each magnetic field line. The electric field is also described by $\mathbf{E} = -\Omega_F \nabla \Psi$, which means that each magnetic field line is equi-potential, and Ω_F corresponds to the potential difference between the field lines. The plasma in the magnetosphere sustains $\rho = (1/4\pi) \nabla \cdot \mathbf{E}$, which produces the electric field in the similar manner to the star.

Equation (3) is satisfied in the whole system we now consider including the inside of the star, as long as there is no region where $\mathbf{E} \cdot \mathbf{B} \neq 0$, i.e., no gap. Comparing it with equation (1), one obtains

$$\Omega_F = \Omega_s. \quad (5)$$

This means that the stellar rotation generates the potential differences in the magnetosphere, i.e., the origin of the electromotive force for pulsar winds is ascribed to the rotation of the stellar matter. For the rigid rotation of the star, Ω_F is constant in the whole system.

It is interesting that the plasma enhances the strength of the electric field across the magnetic field, although it screens that along the magnetic field (satisfying $\mathbf{E} \cdot \mathbf{B} = 0$). In fact, in the plasma-filled case for the dipole magnetic field, which we have considered, one has from equation (3)

$$E_r = \mu \Omega_F \frac{\sin^2 \theta}{r^2}, \quad E_\theta = -\mu \Omega_F \frac{2 \sin \theta \cos \theta}{r^2}, \quad (6)$$

in terms of the spherical coordinates (r, θ, φ) , where μ is the magnetic dipole moment. In the vacuum case, the electric field has quadrupole shape (Goldreich & Julian 1969)

$$E_r = -\mu \Omega_F r_s^2 \frac{3 \cos^2 \theta - 1}{r^4}, \quad E_\theta = -\mu \Omega_F r_s^2 \frac{2 \sin \theta \cos \theta}{r^4}, \quad (7)$$

where r_s is the radius of the star. It is obvious that the electric field is stronger in the plasma-filled case for $r > r_s$.

Let us consider the particle motions in the magnetosphere. Since the energy density is dominated by the electromagnetic field, the particles move via the $\mathbf{E} \times \mathbf{B}$ drifts. For the dipole magnetic field and the associated electric field shown above, this motion is in the direction of φ . It carries the drift currents, but does not produce B_φ . The drift velocity is written by using equation (3) as

$$\mathbf{v}_d = \varpi \Omega_F \mathbf{e}_\varphi - \varpi \Omega_F \frac{B_\varphi}{B^2} \mathbf{B}. \quad (8)$$

As long as $B_\varphi = 0$, one has $\mathbf{v}_d = \varpi \Omega_F \mathbf{e}_\varphi$. Because $\Omega_F = \Omega_s$, the particles co-rotate with the star. The drift current is $J_\varphi = \rho \varpi \Omega_s$. Now one can calculate the charge density in the magnetosphere at $\varpi < 1/\Omega_F$ as

$$\rho = \frac{1}{4\pi} \nabla \cdot \mathbf{E} = \frac{-\Omega_s B_z}{2\pi(1 - \varpi^2 \Omega_s^2)} \approx \frac{-\Omega_s B_z}{2\pi}, \quad (9)$$

This implies that $\rho < 0$ (> 0) in the region where $B_z > 0$ (< 0).

2.2 Poloidal Current Structure

The co-rotation of the particles cannot be maintained outside the light cylinder at $\varpi = \varpi_{lc} \equiv 1/\Omega_F$. The poloidal electric currents must flow. The poloidal currents produce B_φ , which prevents the particle speeds from exceeding the light speed (see equation 8). The particles must flow out along the magnetic field lines which cross the light cylinder. Those magnetic field lines must be open, because of the symmetry with respect to the equatorial plane. The charge density distribution (equation 9) and the particle outflow imply that the poloidal electric currents flow towards the northern and southern poles of the star and flow out from the light cylinder around the equatorial plane. Therefore one finds $B_\varphi < 0$ (> 0) in the main body of the outflow region (i.e., the open field line region) in the northern (southern) hemisphere.

According to equation (8), one has $v_{d,\varphi} = (1 - B_\varphi^2/B^2) \varpi \Omega_F$, and thus it is reasonable that $|B_\varphi| \sim |\mathbf{B}_p|$ around the light cylinder. One might consider that such a strong B_φ is produced by the poloidal currents flowing due to the effects of the particle inertia around the light cylinder, but this is not the case, because the particle energy density is still much smaller than the electromagnetic field energy density around the light cylinder, as seen by the MHD theory (cf., Beskin 2010; Toma & Takahara 2013). B_φ must be produced by the poloidal currents which are driven by the matter-dominated star. The outflows of the positive (negative) charges from the high (low) potential region in the star result in the net electric field $\mathbf{E} + \mathbf{V} \times \mathbf{B} \neq 0$ in the direction of $-\mathbf{E}$, which continues driving the poloidal currents and supplying the positive (negative) charges to the high (low) potential region.

The currents flowing in the direction of $-\mathbf{E}$ in the star generates the poloidal component of the Poynting flux $\mathbf{S}_p = \mathbf{E} \times \mathbf{B}_\varphi / 4\pi = -\Omega_F \varpi B_\varphi \mathbf{B}_p / 4\pi$, as described by

$$\begin{aligned} \nabla \cdot \mathbf{S}_p &= -\mathbf{E} \cdot \mathbf{J}_p = (\mathbf{V}_\varphi \times \mathbf{B}_p) \cdot \mathbf{J}_p \\ &= -(\mathbf{J}_p \times \mathbf{B}_p) \cdot \mathbf{V}_\varphi. \end{aligned} \quad (10)$$

This equation also means that the Lorentz force $\mathbf{J}_p \times \mathbf{B}_p$, being in the direction of $-\mathbf{V}_\varphi$, decelerates the stellar rotation as a feedback of the Poynting flux generation. In this way, the rotating star keeps generating the electromotive force (equation 5), driving the poloidal electric currents, and generating the outward Poynting flux.

Since $|B_\varphi| \sim |\mathbf{B}_p|$ is expected around the light cylinder, one may estimate $|\mathbf{S}_p| \sim B_{p,lc}^2 / 4\pi$, where $B_{p,lc}$ is the strength of the poloidal magnetic field at the light cylinder. The dipole field implies $B_{p,lc} \sim B_{p,s} (\varpi_{lc}/r_s)^{-3}$, where $B_{p,s}$ is the strength of the poloidal magnetic field at the stellar surface. Then the electromagnetic luminosity is roughly estimated as

$$L \sim 4\pi r_{lc}^2 |\mathbf{S}_p| \sim B_{p,s}^2 \Omega_s^4 r_s^6. \quad (11)$$

Here the condition $|B_\varphi| \sim |\mathbf{B}_p|$ around the light cylinder is equivalent to the estimate of the total current I flowing towards the star. In fact, the order of the current density is probably $J_p \sim |\rho|c$, and then $I \sim J_p A$, where A is the area of the stellar surface into which the currents flow, and estimated to be $A \simeq \pi r_s^2 \Omega_s$ (Goldreich & Julian 1969). The electromagnetic luminosity is also calculated by $L \sim 2I\Phi$, where the potential difference $\Phi \sim B_{p,s} r_s^3 \Omega_s^2$, which is con-

sistent with equation (11). (The factor 2 comes from the contributions from the northern and southern hemispheres.)

The poloidal currents must cross the poloidal magnetic field lines in the direction of \mathbf{E} outside the star for making closed circuits, which accelerates the particles via the $\mathbf{J}_p \times \mathbf{B}_\varphi$ force and then converts the Poynting flux to the particle kinetic energy flux. In this paper we do not discuss the particle acceleration mechanism in detail (see Beskin 2010; Toma & Takahara 2013, and references therein).

3 ELECTRODYNAMICS IN KERR SPACE-TIME

We briefly summarize the geometrical properties of Kerr space-time and the electrodynamics in order to define the various physical quantities used in this paper. We follow the definitions and formulations of Komissarov (2004a) except for keeping 4π in Maxwell equations. We adopt the units of $c = 1$ and $GM = 1$, where M is the BH mass. For such units, the gravitational radius $r_g = GM/c^2 = 1$.

3.1 The 3+1 Decomposition of Space-time

The space-time metric can be generally written as

$$ds^2 = g_{\mu\nu} dx^\mu dx^\nu = -\alpha^2 dt^2 + \gamma_{ij} (\beta^i dt + dx^i) (\beta^j dt + dx^j), \quad (12)$$

where α is called the lapse function, β^i the shift vector, and γ_{ij} the three-dimensional metric tensor of the space-like hypersurfaces. The hypersurfaces are regarded as the absolute space at different instants of time t (cf. Thorne et al. 1986). For Kerr space-time, $\partial_t g_{\mu\nu} = \partial_\varphi g_{\mu\nu} = 0$. These correspond to the existences of the Killing vector fields ξ^μ and χ^μ . In the coordinates (t, φ, r, θ) , $\xi^\mu = (1, 0, 0, 0)$ and $\chi^\mu = (0, 1, 0, 0)$.

The local fiducial observer (FIDO; Bardeen et al. 1972; Thorne et al. 1986), whose world line is perpendicular to the absolute space, is described by the coordinate four-velocity

$$n^\mu = \left(\frac{1}{\alpha}, \frac{-\beta^i}{\alpha} \right), \quad n_\mu = g_{\mu\nu} n^\nu = (-\alpha, 0, 0, 0). \quad (13)$$

The angular momentum of this observer is $n \cdot \chi = g_{\mu\nu} n^\mu \chi^\nu = n_\varphi = 0$, and thus FIDO is also a zero angular momentum observer (ZAMO; Thorne et al. 1986). Note that the FIDO frame is not inertial, but it can be used as a convenient orthonormal basis to investigate the local physics (Thorne et al. 1986; Punsly & Coroniti 1990; Punsly 2008).

In the Boyer-Lindquist (BL) coordinates (t, φ, r, θ) (see Appendix A), FIDOs rotate with the coordinate angular velocity

$$\Omega \equiv \frac{d\varphi_{\text{FIDO}}}{dt} = -\beta^\varphi > 0, \quad (14)$$

which is in the same direction as the BH. The BL coordinates have the well-known coordinate singularity ($g_{rr} = \infty$) at the event horizon. The radius of the event horizon is $r_H = 1 + \sqrt{1 - a^2}$. The Killing vector ξ^μ is space-like in the ergosphere, where $\xi^2 = g_{tt} = -\alpha^2 + \beta^2 > 0$. The radius of the outer boundary of the ergosphere (i.e., the stationary limit) is $r_{\text{es}} = 1 + \sqrt{1 - a^2 \cos^2 \theta}$. At infinity, this space-time asymptotes to the flat one. The shapes of the event horizon and the ergosphere are shown in Fig. 1.

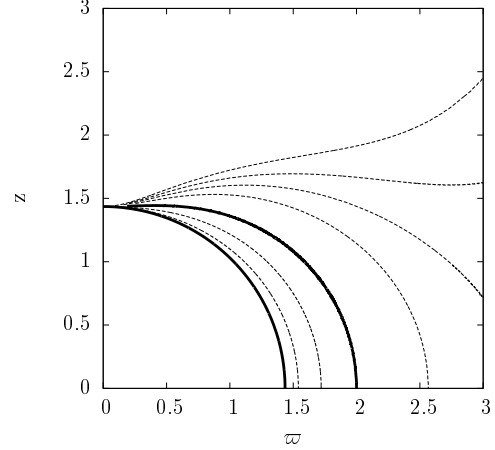


Figure 1. The event horizon (inner thick line) and the outer boundary of the ergosphere (outer thick line) of Kerr space-time. The thin lines represent $\Omega - \alpha/\sqrt{\gamma_{\varphi\varphi}} = 0.2, 0.1, -0.1, -0.14, -0.17, -0.2$ in the BL coordinates in the order of increasing r . The line of $\Omega - \alpha/\sqrt{\gamma_{\varphi\varphi}} = 0$ is identical to the outer thick line. The spin parameter is set to be $a = 0.9$.

The Kerr-Schild (KS) coordinates have no coordinate singularity at the event horizon. However, the KS spatial coordinates are no longer orthogonal ($\gamma_{r\varphi} \neq 0$; see Appendix A), and then one should be cautious for examining the spatial structure of the electromagnetic field by using the KS coordinates.

3.2 The 3+1 Electrodynamics

In order to study the test electromagnetic field in Kerr space-time, we adopt the 3+1 electrodynamics of the version which was developed by Komissarov (2004a) (see also Landau & Lifshitz 1975; Komissarov 2009, and references therein).² The covariant Maxwell equations $\nabla_\nu {}^*F^{\mu\nu} = 0$ and $\nabla_\nu F^{\mu\nu} = 4\pi I^\mu$ are reduced to

$$\nabla \cdot \mathbf{B} = 0, \quad \partial_t \mathbf{B} + \nabla \times \mathbf{E} = 0, \quad (15)$$

$$\nabla \cdot \mathbf{D} = 4\pi\rho, \quad -\partial_t \mathbf{D} + \nabla \times \mathbf{H} = 4\pi\mathbf{J}, \quad (16)$$

where $\nabla \cdot \mathbf{C}$ and $\nabla \times \mathbf{C}$ denote $(1/\sqrt{\gamma})\partial_i(\sqrt{\gamma}C^i)$ and $e^{ijk}\partial_j C_k$, respectively, and $e^{ijk} = (1/\sqrt{\gamma})\epsilon^{ijk}$ is the Levi-Civita pseudo-tensor of the absolute space. The condition of zero electric and magnetic susceptibilities for general fully-ionized plasmas leads to following constitutive equations,

$$\mathbf{E} = \alpha\mathbf{D} + \boldsymbol{\beta} \times \mathbf{B}, \quad (17)$$

$$\mathbf{H} = \alpha\mathbf{B} - \boldsymbol{\beta} \times \mathbf{D}, \quad (18)$$

where $\mathbf{C} \times \mathbf{F}$ denotes $e^{ijk}C_j F_k$. At infinity, $\alpha = 1$ and $\boldsymbol{\beta} = 0$, so that $\mathbf{E} = \mathbf{D}$ and $\mathbf{H} = \mathbf{B}$. Here \mathbf{D} , \mathbf{B} , and ρ are the electric field, magnetic field, and charge density as measured by FIDOs, respectively (see Appendix A for more details). The current \mathbf{J} is related to the current as measured by FIDOs, \mathbf{j} , as

² Thorne & MacDonald (1982) and Thorne et al. (1986) developed the 3+1 electrodynamics of the version without introducing \mathbf{E} or \mathbf{H} , and showed some of the expressions in this paper, such as equations (22) and (29).

$$\mathbf{J} = \alpha \mathbf{j} - \rho \boldsymbol{\beta}. \quad (19)$$

The covariant energy-momentum equation of the electromagnetic field $\nabla_\nu T'_\mu = -F_{\mu\nu} I^\nu$ gives us the energy equation as

$$\partial_t \left[\frac{1}{8\pi} (\mathbf{E} \cdot \mathbf{D} + \mathbf{B} \cdot \mathbf{H}) \right] + \nabla \cdot \left(\frac{1}{4\pi} \mathbf{E} \times \mathbf{H} \right) = -\mathbf{E} \cdot \mathbf{J}, \quad (20)$$

where $\mathbf{C} \cdot \mathbf{F}$ denotes $C^i F_i$, and the angular momentum equation as

$$\partial_t \left[\frac{1}{4\pi} (\mathbf{D} \times \mathbf{B}) \cdot \mathbf{m} \right] + \nabla \cdot \left[-(\mathbf{E} \cdot \mathbf{m}) \mathbf{D} - (\mathbf{H} \cdot \mathbf{m}) \mathbf{B} + \frac{1}{2} (\mathbf{E} \cdot \mathbf{D} + \mathbf{B} \cdot \mathbf{H}) \mathbf{m} \right] = -(\rho \mathbf{E} + \mathbf{J} \times \mathbf{B}) \cdot \mathbf{m}, \quad (21)$$

where $\mathbf{m} = \partial_\varphi$. From these equations, one can find the energy density, energy flux, angular momentum density, and angular momentum flux.

3.3 Steady Axisymmetric Electromagnetic Field in the Vacuum

Before investigating the plasma-filled magnetosphere in Kerr space-time, the properties of the electromagnetic field in the vacuum (i.e., no plasma) are summarized. Wald (1974) derived the solution of a steady, axisymmetric, vacuum test electromagnetic field in Kerr space-time for which the magnetic field is uniform, parallel to the rotation axis, at infinity in an elegant way by utilizing the fact that ξ^μ and χ^μ generate a solution of Maxwell equations (see Appendix A). For this solution, the poloidal \mathbf{D} field is non-zero. This may be understood by considering $\nabla \times \mathbf{E} = \nabla \times (\alpha \mathbf{D} + \boldsymbol{\beta} \times \mathbf{B}) = 0$. Since $\nabla \times (\boldsymbol{\beta} \times \mathbf{B}) \neq 0$ generally, one has $\nabla \times (\alpha \mathbf{D}) \neq 0$. This \mathbf{D} field is produced by the charges at the event horizon and at infinity. Note that $\mathbf{D} \cdot \mathbf{B} \neq 0$ for this solution.

$\nabla \times \mathbf{E} = 0$ implies $E_\varphi = 0$, and $\nabla \times \mathbf{H} = 0$ tells us $H_\varphi = 0$. Then the poloidal components of the energy and angular momentum fluxes are zero. These properties are the same as those for the pulsar in the vacuum.

4 KERR BLACK HOLE MAGNETOSPHERE

Now we examine the steady, axisymmetric, test electromagnetic field in Kerr space-time in which the plasma is filled. As a preparation for the discussion on the unipolar induction of rotating black holes (in Section 5), we summarize the general properties of the electromagnetic field in Section 4.1. In Section 4.2, we study the particle motions as viewed by FIDOs. This study provides a conclusion that $D^2 > B^2$ is the necessary and sufficient condition for driving the electric currents to flow across the poloidal \mathbf{B} field lines.

4.1 Electromagnetic Field

We consider the Kerr BH magnetosphere under the following assumptions: (1) The poloidal \mathbf{B} field produced by the external electric currents is penetrating the ergosphere. (2) The plasma in the BH magnetosphere is dilute and collisionless, but its number density is high enough to screen the electric field along the \mathbf{B} field lines, i.e., $\mathbf{D} \cdot \mathbf{B} = 0$. The energy density of the particles is much smaller than that of the electromagnetic field. (3) The gravitational force is

negligible compared with the Lorentz force. (The gravitational force overwhelms the Lorentz force in a region very close to the event horizon (Punsly 2008), but the physical condition in that region hardly affects its exterior.) These assumptions are the same as those for the pulsar case. One big difference is that there is no matter-dominated region on which the \mathbf{B} field is anchored (see Section 1). As a result, the determination of Ω_F is not so simple as the pulsar case.

In terms of the vector potential, one can write $\mathbf{B} = \nabla \times \mathbf{A}$ (Komissarov 2004a). Thus one finds

$$B^r = \frac{1}{\sqrt{\gamma}} \partial_\theta \Psi, \quad B^\theta = -\frac{1}{\sqrt{\gamma}} \partial_r \Psi, \quad (22)$$

where we have defined $\Psi \equiv A_\varphi$. It is easily shown that $B^i \partial_i \Psi = 0$, which means that Ψ is constant along each \mathbf{B} field line.

The condition $\mathbf{D} \cdot \mathbf{B} = 0$ and equation (17) lead to $\mathbf{E} \cdot \mathbf{B} = 0$. Taking account of $E_\varphi = 0$, one can write

$$\mathbf{E} = -\boldsymbol{\omega} \times \mathbf{B}, \quad \boldsymbol{\omega} = \Omega_F \mathbf{m}. \quad (23)$$

Substituting this equation into $\nabla \times \mathbf{E} = 0$ and $\nabla \cdot \mathbf{B} = 0$, one obtains

$$B^i \partial_i \Omega_F = 0. \quad (24)$$

That is, Ω_F is constant along each \mathbf{B} field line. The \mathbf{E} field is also described by $E_i = -\Omega_F \partial_i \Psi$, which means that each \mathbf{B} field line is equi-potential, and Ω_F corresponds to the potential difference between the field lines. These properties are the same as those in the pulsar case, discussed in Section 2.

In the steady, axisymmetric state, the angular momentum equation (21) is reduced to

$$\nabla \cdot \left(-\frac{H_\varphi}{4\pi} \mathbf{B}_p \right) = B^i \partial_i \left(-\frac{H_\varphi}{4\pi} \right) = -(\mathbf{J}_p \times \mathbf{B}_p) \cdot \mathbf{m}. \quad (25)$$

The energy equation (20) is reduced to

$$\nabla \cdot \left(-\Omega_F \frac{H_\varphi}{4\pi} \mathbf{B}_p \right) = B^i \partial_i \left(-\Omega_F \frac{H_\varphi}{4\pi} \right) = -\mathbf{E} \cdot \mathbf{J}_p, \quad (26)$$

which can be deduced by equation (25) together with equations (23) and (24). These equations imply that H_φ is generated by the poloidal currents which have the component perpendicular to the poloidal \mathbf{B} field, and then the poloidal component of the Poynting flux $-\Omega_F H_\varphi \mathbf{B}_p / (4\pi)$ is non-zero when $\Omega_F \neq 0$. We note that $\Omega_F = -F_{t\theta} / F_{\varphi\theta}$ and $H_\varphi = *F_{t\varphi}$ are the same in the BL and KS coordinates (Komissarov 2004a).

4.2 Poloidal Currents

Komissarov (2004a) argues that the poloidal currents can have the component perpendicular to the poloidal \mathbf{B} field in the region where $D^2 > B^2$, by utilizing a specific Ohm's law (or some effective resistivity). Here we prove this to be valid by examining particle motions in the electromagnetic fields more generally, without relying on the Ohm's law.

We treat the particle motion as viewed by FIDOs. They can use a convenient local orthonormal basis for which the space-time metric is diagonal and one can investigate local, instantaneous particle motions under the Lorentz force as special relativistic dynamics. In fact, the equation of a particle motion as viewed by FIDOs (either BL or KS FIDOs) is

$$\frac{d\hat{u}_i}{dt} = \frac{q}{m}(\hat{D}_i + \epsilon_{ijk}\hat{v}^j\hat{B}^k), \quad (27)$$

as shown in Appendix B. Here \mathbf{u} , \mathbf{v} , q , and m are the four-velocity, three-velocity, charge, and mass of a particle, respectively, and \hat{C}_i denotes the vector component in respect of the FIDO's orthonormal basis, i.e., $\hat{C}_i = C_\mu e_i^\mu$ (see Appendix A).³ Note that the FIDO frame is not inertial and a particle feels the gravitational force, although we assume that it is negligible compared with the Lorentz force. In this equation \hat{D}_i and \hat{B}^i appear as the electric and magnetic fields as viewed by FIDOs, respectively, as expected. The assumption $\mathbf{D} \cdot \mathbf{B} = 0$ is equivalent to $\hat{\mathbf{D}} \cdot \hat{\mathbf{B}} = 0$, because $D^\mu B_\mu$ is a scalar and $\hat{D}^t = D^t = 0$.

When $D^2 < B^2$ is satisfied (which is equivalent to $\hat{D}^2 < \hat{B}^2$), the charged particles freely move along the $\hat{\mathbf{B}}$ field line and/or drift in the direction of $\hat{\mathbf{D}} \times \hat{\mathbf{B}}$. Effectively one has $\hat{\mathbf{u}}_+ \cdot \hat{\mathbf{D}} = \hat{\mathbf{u}}_- \cdot \hat{\mathbf{D}} = 0$, where \mathbf{u}_+ and \mathbf{u}_- denote the four-velocities of positively and negatively charged particles, respectively. This equation is valid as long as the plasma is dilute and any particle collisions which induce $\hat{\mathbf{u}}_+ \cdot \hat{\mathbf{D}} \neq 0$ or $\hat{\mathbf{u}}_- \cdot \hat{\mathbf{D}} \neq 0$ are ineffective. In the coordinate basis, one has $\mathbf{u}_+ \cdot \mathbf{D} = \mathbf{u}_- \cdot \mathbf{D} = 0$, since $u_\mu D^\mu$ is a scalar and $\hat{D}^t = D^t = 0$. Then by considering $u^i = u^t v^i$, one has $\mathbf{v}_+ \cdot \mathbf{D} = \mathbf{v}_- \cdot \mathbf{D} = 0$. As a result, the motions of the charged particles can carry only the electric currents satisfying $\mathbf{J}_p \cdot \mathbf{D} = 0$ and $\mathbf{J}_p \parallel \mathbf{B}_p$.

If $D^2 > B^2$ is realized (which is equivalent to $\hat{D}^2 > \hat{B}^2$), then the positively (negatively) charged particles are forced to move in the direction of $\hat{\mathbf{D}}$ ($-\hat{\mathbf{D}}$) (cf. Landau & Lifshitz 1975), i.e., $\hat{\mathbf{u}}_+ \cdot \hat{\mathbf{D}} > 0$ and $\hat{\mathbf{u}}_- \cdot \hat{\mathbf{D}} < 0$. Then one has $\mathbf{u}_+ \cdot \mathbf{D} > 0$ and $\mathbf{u}_- \cdot \mathbf{D} < 0$ in the coordinate basis, which lead to $\mathbf{v}_+ \cdot \mathbf{D} > 0$ and $\mathbf{v}_- \cdot \mathbf{D} < 0$ since $u^t > 0$. Therefore, the particle motions can carry $\mathbf{J}_p \parallel \mathbf{D}$. This implies $\mathbf{J}_p \perp \mathbf{B}_p$. The force-free approximation $F_{\mu\nu} I^\nu = 0$ (i.e., $\rho \mathbf{E} + \mathbf{J} \times \mathbf{B} = 0$) is violated in this case, since $E_\varphi = 0$.

In summary, $D^2 > B^2$ is the necessary and sufficient condition for driving the electric currents to flow across the poloidal \mathbf{B} field lines (and then obtaining $H_\varphi \neq 0$) under our assumptions (1)–(3) listed in Section 4.1.

5 UNIPOLAR INDUCTION OF KERR BLACK HOLES

We discuss the unipolar induction process in the Kerr BH magnetosphere where the poloidal \mathbf{B} field lines threading the ergosphere are open, i.e., crossing the outer light surface. We mainly utilize the BL coordinates rather than the KS ones in this section.

The light surfaces are defined as follows. In the BL coordinates, when $\hat{B}_\varphi = B_\varphi = 0$, the coordinate angular velocity of the drift motion is Ω_F , as deduced in Appendix B. The light surfaces are the surfaces where the four-velocity of a particle which is rotating with the coordinate angular velocity Ω_F becomes null, i.e., $f(\Omega_F, r, \theta) = 0$, where we have defined

$$f(\Omega_F, r, \theta) \equiv (\xi + \Omega_F \chi)^2 = -\alpha^2 + \gamma_{\varphi\varphi}(\Omega_F - \Omega)^2. \quad (28)$$

³ The quantities $\hat{\mathbf{E}}$ and $\hat{\mathbf{B}}$ used in Komissarov (2004a) are identical to \mathbf{D} and \mathbf{B} . The FIDO's orthonormal basis is not utilized for discussion in Komissarov (2004a).

There can be two light surfaces. One has $\Omega_F - \Omega = \alpha/\sqrt{\gamma_{\varphi\varphi}}$ at the outer light surface (where $\Omega < \Omega_F$), while $\Omega_F - \Omega = -\alpha/\sqrt{\gamma_{\varphi\varphi}}$ at the inner light surface (where $\Omega > \Omega_F$).

From the condition $\mathbf{D} \cdot \mathbf{B} = 0$, equations (17) and (23) lead to

$$\mathbf{D} = -\frac{1}{\alpha}(\boldsymbol{\omega} + \boldsymbol{\beta}) \times \mathbf{B}. \quad (29)$$

Calculating $D^2 \equiv D^i D_i$, one obtains in the BL coordinates

$$D^2 = \frac{1}{\alpha^2}(\Omega_F - \Omega)^2 B_p^2, \quad (30)$$

where $B_p^2 \equiv B^r B_r + B^\theta B_\theta$. This equation can be rewritten by using equation (28) (cf. Komissarov 2004a)

$$(B^2 - D^2)\alpha^2 = -B^2 f(\Omega_F, r, \theta) + \frac{1}{\alpha^2}(\Omega_F - \Omega)^2 H_\varphi^2, \quad (31)$$

where we have used $H_\varphi = \alpha B_\varphi$ (see equation 18). This equation is useful for the following discussion.

5.1 Origin of the electromotive force

We show that there is no steady, axisymmetric state with $\Omega_F = 0$ and $H_\varphi = 0$ for the \mathbf{B} field lines threading the ergosphere. The condition $\Omega_F = 0$ means $\mathbf{E} = 0$, and $\mathbf{D} = (-1/\alpha)\boldsymbol{\beta} \times \mathbf{B}$. Equation (31) is reduced to

$$(B^2 - D^2)\alpha^2 = B^2(\alpha^2 - \beta^2). \quad (32)$$

In the ergosphere, where $\alpha^2 - \beta^2 < 0$, one has $D^2 > B^2$. Note that $B^2 - D^2 = F_{\mu\nu} F^{\mu\nu}/2$ is a scalar, and thus $B^2 - D^2 < 0$ is valid also in the KS coordinates. The \mathbf{D} field stronger than the \mathbf{B} field drives the poloidal currents to flow across the poloidal \mathbf{B} field lines, as discussed in Section 4.2. These poloidal currents generate H_φ (equation 25). Therefore, the state with $\Omega_F = 0$ and $H_\varphi = 0$ cannot be maintained.

The poloidal currents (i.e., the charged particle flows) across the poloidal \mathbf{B} field lines due to the strong \mathbf{D} field in the ergosphere change the charge density distribution. This reduces the strength of the \mathbf{D} field. (We show the charge density distribution calculated for the Wald \mathbf{B}_p field in Appendix C, which might be helpful for understanding the reduction of the \mathbf{D} field strength by the charged particle flows across the poloidal \mathbf{B} field lines.) Then equation (30) implies that $\Omega_F > 0$ is realized and one finds a non-zero \mathbf{E} field.

From this argument, we can conclude that the origin of the electromotive force is ascribed to the ergosphere in the unipolar induction of the BH magnetosphere with $\mathbf{D} \cdot \mathbf{B} = 0$.

The generation of such a strong \mathbf{D} field may be understood as a phenomenon similar to the pulsar case. In the vacuum case, we can straightforwardly calculate D^2/B^2 by using the Wald solution (see Appendix A), and find that the region where $D^2 > B^2$ is only in the vicinity of the event horizon at the equatorial plane, as shown in Fig. 2. In contrast, one has $D^2/B^2 = \beta^2/\alpha^2$ in the plasma-filled case with $\Omega_F = 0$ and $H_\varphi = 0$ (equation 32), which is larger than unity in the entire ergosphere (see the dot-dashed line in Fig. 2). The enhancement of the electric field in the plasma-filled case compared to the vacuum case is quite similar to the pulsar case (see equations 6 and 7 in Section 2.1). The charge distribution of the plasma screen the \mathbf{D} field component along the \mathbf{B} field but enhances the total strength of the \mathbf{D} field. Note that the condition $D^2 > B^2$

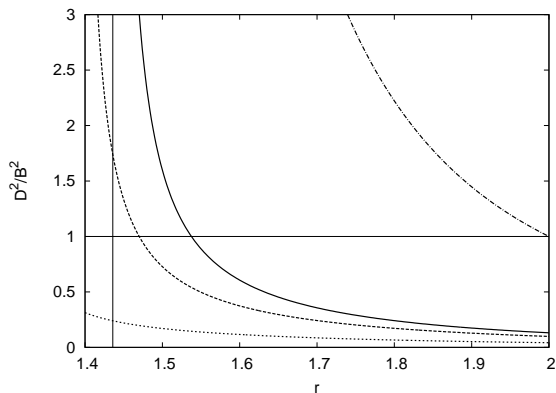


Figure 2. D^2/B^2 calculated for the Wald vacuum solution in the BL coordinates, as functions of r for $\theta = \pi/2$ (solid), 0.45π (dashed), and 0.4π (dotted). The spin parameter is set as $a = 0.9$. For comparison, $D^2/B^2 (= \beta^2/\alpha^2)$ in the plasma-filled case with $\Omega_F = 0$ and $H_\varphi = 0$ for $\theta = \pi/2$ is plotted by the dot-dashed line. The vertical line represents the event horizon radius $r_H = 1.436$. The outer boundary of the ergosphere is $r_{es} = 2$ for $\theta = \pi/2$.

is not due to a shortage of the number of charged particles like the gap with non-zero electric field *along* the magnetic field lines (Blandford & Znajek 1977; Beskin et al. 1992; Hirohani & Okamoto 1998), but rather, it arises due to a sufficiency of the charged particles sustaining $\mathbf{D} \cdot \mathbf{B} = 0$.

The divergence of D^2/B^2 near the event horizon in Fig. 2 is not physical, just due to the BL coordinate singularity. In Appendix A, we calculate D^2/B^2 in the KS coordinates, which does not show any divergence (see Fig. A1).

We also find that no \mathbf{B} field lines can have the condition of $\Omega_F = 0$ and $H_\varphi \neq 0$. Along such \mathbf{B} field lines, the poloidal electromagnetic angular momentum flux is non-zero, but the poloidal Poynting flux is zero (see equations 25 and 26). The current closure requires that such a \mathbf{B} field line should have a part where the poloidal currents cross this field line. Focusing on the currents crossing the field line at the far zone, one finds that the $\mathbf{J}_p \times \mathbf{B}_\varphi$ force acts on the matter, converting the poloidal momentum flux of the electromagnetic field to that of the matter. The matter should also gain the poloidal energy flux from the electromagnetic field, which conflicts with the condition of $\Omega_F = 0$. Therefore, the state with $\Omega_F = 0$ and $H_\varphi \neq 0$ must not be realized.

5.2 Maintenance of the poloidal currents

As discussed above, the condition $\Omega_F > 0$ is inevitably satisfied for all the \mathbf{B} field lines threading the ergosphere in the steady, axisymmetric state. This condition leads to the azimuthal drift motions of the particles at the far zone, similar to the pulsar case. For the *open* \mathbf{B} field lines that we consider, they must have the condition $B_\varphi = H_\varphi/\alpha \neq 0$ so that the azimuthal drift speeds do not exceed the light speed. Therefore, the open \mathbf{B} field lines threading the ergosphere will be forced to have the condition $\Omega_F > 0$ and $H_\varphi \neq 0$.

We have seen that H_φ is generated by the poloidal currents driven to flow across the poloidal \mathbf{B} field line. Then the field line should have a part where $D^2 > B^2$ in the ergosphere (see also Section 5.3 below) in order to maintain the poloidal currents, although those currents reduce the

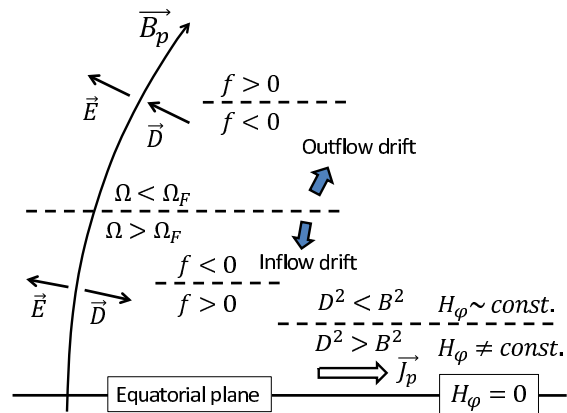


Figure 3. Electromagnetic structure in the northern hemisphere along a \mathbf{B} field line threading the equatorial plane in the ergosphere. The direction of the \mathbf{D} field changes at the point of $\Omega = \Omega_F$. This corresponds to the change of the $\mathbf{D} \times \mathbf{B}_\varphi$ drift direction. The current crossing region is the region of $D^2 > B^2$, where H_φ is not constant, and located below the inner light surface ($f(\Omega_F, r, \theta) = 0$).

strength of the \mathbf{D} field (leading to a larger value of Ω_F). Therefore, the value of Ω_F will be regulated so that $\Omega_F > 0$ and the \mathbf{B} field line keeps having a part where $D^2 > B^2$.

It should be noted that the ergosphere is causally connected to the region around the outer light surface, which is inside the outer fast magnetosonic surface (cf., Punsly 2008; Beskin 2010; Toma & Takahara 2012). Thus the steady state with $\Omega_F > 0$ and $H_\varphi \neq 0$ can be established in principle, although more quantitative analyses on the stability of this state are needed.

If we have any \mathbf{B} field lines which penetrate the ergosphere but are not open, e.g., field lines having the cylindrical shapes and not crossing the outer light surfaces, they can be in the steady state with $\Omega_F > 0$ and $H_\varphi = 0$. Such field lines do not have a region where $D^2 > B^2$ (i.e., Ω_F is larger than the case of $H_\varphi \neq 0$).

5.3 B fields threading the equatorial plane

Let us call the region where $D^2 > B^2$ and then the poloidal currents are driven to flow across the poloidal \mathbf{B} field line “current crossing region.” In the case of $\Omega_F = 0$ and $H_\varphi = 0$, the current crossing region has been found to be the ergosphere in Section 5.1. Where is the current crossing region in the case of $\Omega_F > 0$ and $H_\varphi \neq 0$? Here we focus on an open \mathbf{B} field line *threading the equatorial plane* in the ergosphere, showing a self-consistent electromagnetic structure along such a field line and pinning down the region where $D^2 > B^2$.

First, since $\Omega_F > 0$, there is a point where $\Omega = \Omega_F$ for each field line. One has $\mathbf{D} \cdot \mathbf{E} < 0$ below this point, while $\mathbf{D} \cdot \mathbf{E} > 0$ above this point, as illustrated in Fig. 3. The point of $\Omega = \Omega_F$ is located between the outer light surface (where $\Omega_F - \Omega = \alpha/\sqrt{\gamma_{\varphi\varphi}} > 0$) and the inner light surface (where $\Omega_F - \Omega = -\alpha/\sqrt{\gamma_{\varphi\varphi}} < 0$). We plot the contour of $\Omega - \alpha/\sqrt{\gamma_{\varphi\varphi}}$ in Fig. 1, which shows that $\Omega - \alpha/\sqrt{\gamma_{\varphi\varphi}}$ is positive only in the ergosphere. Thus $\Omega_F > 0$ requires that the inner light surface is located in the ergosphere.

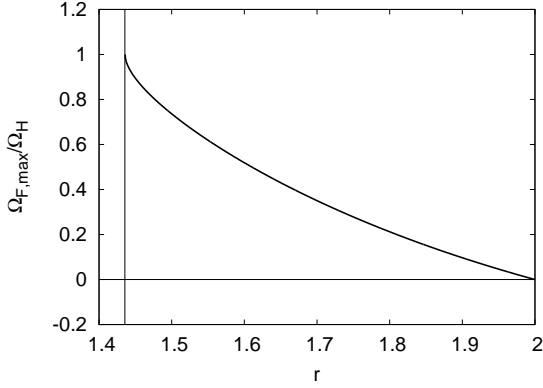


Figure 4. $\Omega_{F,\max}/\Omega_H$ for the \mathbf{B} field lines threading the equatorial plane in the ergosphere as functions of r on the equatorial plane. The spin parameter is set as $a = 0.9$. The vertical line represents $r_H = 1.436$. The radius of the outer boundary of the ergosphere is $r_{\text{es}} = 2$.

Because of the symmetry, $H_\varphi = 0$ on the equatorial plane. The current crossing region must include the equatorial plane, and H_φ is generated in this region (see equation 25). Equation (31) implies that $D^2 > B^2$ is satisfied in the region of $f(\Omega_F, r, \theta) > 0$. Therefore, *the current crossing region must be below the inner light surface, which is within the ergosphere*. Above the current crossing region, $D^2 < B^2$ is satisfied and $H_\varphi \sim \text{const.}$ (Here we do not consider the region where the currents flow across the poloidal \mathbf{B} field lines in the direction of \mathbf{E} , i.e., the particle acceleration zone.) We summarize the electromagnetic structure in Fig. 3.

In the current crossing region, one has $\mathbf{D} \cdot \mathbf{E} < 0$, so that $(\mathbf{J}_p \times \mathbf{B}_p) \cdot \mathbf{m} < 0$ and $\mathbf{E} \cdot \mathbf{J}_p < 0$, which generate the poloidal electromagnetic angular momentum and energy fluxes, as seen in equations (25) and (26). Similar to the pulsar case (discussed in Section 2.2), the poloidal currents are driven to flow across the poloidal \mathbf{B} field lines in the direction of $-\mathbf{E}$ in the region where the outward energy flux is generated.

In the main body of the open field line region in the northern (southern) hemisphere, one has $H_\varphi < 0 (> 0)$, i.e., the poloidal currents flow downward (upward). The poloidal particle drift motions in the coordinate basis (which is in the direction of $\mathbf{D} \times \mathbf{B}_\varphi$ as shown in Appendix B) are directed towards infinity in the region of $\Omega < \Omega_F$, while towards the equatorial plane in the region of $\Omega > \Omega_F$. The particles which drift towards the equatorial plane do not pass through the plane but turn to move parallel to the plane due to the strong \mathbf{D} field.

5.4 Range of Ω_F and outflow power

A necessary condition for maintaining the electromagnetic structure along a \mathbf{B} field line threading the equatorial plane in the ergosphere (Fig. 3) is that the size of the current crossing region is finite. In the limit of the infinitesimally thin current crossing region, $D^2 \approx B^2$ on the equatorial plane. Since $H_\varphi = 0$ there, equation (31) implies $f(\Omega_F, r, \theta) \approx 0$. This condition provides the maximum allowed value of Ω_F , i.e., we find the range of possible value of Ω_F as

$$0 < \Omega_F < \Omega_{F,\max} \equiv \left(\Omega - \frac{\alpha}{\sqrt{\gamma_{\varphi\varphi}}} \right) \Big|_{z=0}. \quad (33)$$

The value of $\Omega_{F,\max}$ normalized by the BH angular velocity $\Omega_H = a/(2r_H)$ as a function of r on the equatorial plane is plotted in Fig. 4. Since the poloidal current flows reduce the strength of the \mathbf{D} field, as discussed above, Ω_F is expected to have a value near $\Omega_{F,\max}$.

Fig. 4 implies that Ω_F should be zero for the \mathbf{B} field line threading the ergosphere at $r = r_{\text{es}}$, which we call “last ergospheric field line.” The poloidal currents will not cross this field line, and thus $H_\varphi = 0$ for this field line. The poloidal current circuit can consist of the current flow in the current crossing region, the outward flow along the last ergospheric field line, and the inward flow in the main body of the open field line region (See Fig. 5 and Section 6).

Similar to the pulsar case, it is reasonable that $|\mathbf{B}_\varphi| = |B_\varphi|/\sqrt{\gamma_{\varphi\varphi}} \sim |\mathbf{B}_p|$ around the outer light surface. Then we can have a rough estimate of the poloidal Poynting flux as $|\mathbf{S}_p| = \Omega_F |H_\varphi| |\mathbf{B}_p| / 4\pi \sim B_{p,\text{ls}}^2 / (4\pi)$, where we have used the equations valid at the outer light surface $f(\Omega_F, r, \theta) = -\alpha^2 + \gamma_{\varphi\varphi}(\Omega_F - \Omega)^2 = 0$, $\alpha \sim 1$, and $\Omega \ll \Omega_F$. When the open poloidal magnetic field roughly scales as $B_{p,\text{ls}} \sim B_{p,\text{H}}(r_{\text{ls}}/r_H)^{-2}$ (i.e., monopole-like rather than dipole), where $B_{p,\text{H}}$ is the field strength in the vicinity of the BH and r_{ls} is the radius of the outer light surface, and then one has the luminosity per solid angle as

$$\frac{dL}{d\Omega} \sim r_{\text{ls}}^2 |\mathbf{S}_p| \sim \frac{B_{p,\text{H}}^2 \Omega_F^2 r_H^4}{4\pi} \sim \frac{a^2}{16\pi} \left(\frac{\Omega_F}{\Omega_H} \right)^2 B_{p,\text{H}}^2 r_H^2. \quad (34)$$

Here Ω_F/Ω_H is expected to be $\sim \Omega_{F,\max}/\Omega_H$ (Fig. 4) for the \mathbf{B} field lines threading the equatorial plane in the ergosphere.

6 SUMMARY AND DISCUSSION

We consider the Blandford-Znajek process as the steady unipolar induction process in the Kerr BH magnetosphere in which a collisionless plasma is filled so that $\mathbf{D} \cdot \mathbf{B} = 0$ is sustained and the energy density is dominated by the electromagnetic field. The origin of the electromotive force in this process is the ergosphere, unlike in the pulsar case, in which the origin of the electromotive force is the rotation of the stellar matter (see Section 2). All the open \mathbf{B} field lines threading the ergosphere inevitably keep having a part where the \mathbf{D} field (perpendicular to the \mathbf{B} field) is stronger than the \mathbf{B} field, i.e., $D^2 > B^2$, which drives the poloidal currents to flow across the poloidal \mathbf{B} field lines ($H_\varphi \neq 0$; see equation 25) and give rise to the electromotive force, i.e., $\Omega_F > 0$. In the current crossing region, the currents flow in the direction of $-\mathbf{E}$, which generate the poloidal Poynting flux (see equation 26), similar to the pulsar case. The condition $\mathbf{J}_p \times \mathbf{B}_p \neq 0$ in the current crossing region implies that the force-free approximation cannot be assumed (see Section 4.2). Note that we only assume $\mathbf{D} \cdot \mathbf{B} = 0$, not utilizing the force-free condition $\rho \mathbf{E} + \mathbf{J} \times \mathbf{B} = 0$ in our arguments.

6.1 \mathbf{B} fields threading the horizon

We have shown the self-consistent electromagnetic structure along a \mathbf{B} field line threading the equatorial plane in the ergosphere in Fig. 3. Also for the \mathbf{B} field lines threading the

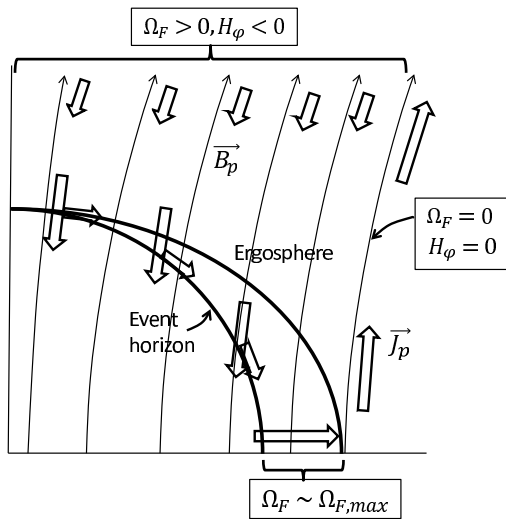


Figure 5. Expected electromagnetic structure of the BH magnetosphere (northern hemisphere). The thin solid arrows represent the poloidal \mathbf{B} field lines, and the open arrows the poloidal currents. See the texts in Sections 5 and 6 for details.

event horizon, the above conclusion on the origin of the electromotive force is applicable, and thus the electromagnetic structure will be similar to Fig. 3, having the current crossing region just outside the horizon. It is not an easy task to solve the whole electromagnetic structure of the BH magnetosphere, but our arguments so far allow us to conjecture that the solution looks like Fig. 5. We describe the poloidal current flows by the open arrows in Fig. 5. Some fraction of the poloidal currents can flow across the horizon, while the remaining fraction flows across the poloidal \mathbf{B} field lines just outside the horizon, generating the poloidal Poynting flux. In the current crossing region around the equatorial plane, the negatively charged particles flow across the horizon. The current circuits will be made for the BH not to charge up in the steady state.

In the membrane paradigm (Thorne et al. 1986; Penna et al. 2013), the force-free condition is assumed to be satisfied except on the membrane (at $r \approx r_H$) covering the horizon, so that all the poloidal currents flow into the membrane (i.e., flow across the horizon for freely falling observers) in the region of the \mathbf{B} field lines threading the horizon. The poloidal currents are then regarded as flowing along the viscous membrane and generating the outward Poynting flux. However, this picture looks unphysical, because the membrane is causally disconnected with its exterior (Punsly & Coroniti 1989; Punsly 2008). The energy equation (26) implies that a region of $\mathbf{E} \cdot \mathbf{J}_p < 0$ has to be causally connected for producing the Poynting flux. Such a region is realized outside the horizon (or the membrane) and within the ergosphere, where the force-free condition is violated.

We have deduced the maximum value of Ω_F , $\Omega_{F,max}$, for the poloidal \mathbf{B} field lines threading the equatorial plane in the ergosphere as shown in Fig. 4. This can be deduced easily by utilizing the symmetry condition on the equatorial plane $H_\varphi = 0$ for equation (31). In contrast, for the poloidal \mathbf{B} field lines threading the horizon, $\Omega_{F,max}$ is difficult to deduce, because $H_\varphi \neq 0$ at the horizon in general. Further-

more, the BL coordinates are not useful for analyzing the condition near the horizon. Equation (29) can be rewritten in the KS coordinates as

$$(B^2 - D^2)\alpha^2 = -B^2 f(\Omega_F, r, \theta) + (\Omega_F B_\varphi + \beta^r B_r)^2, \quad (35)$$

where $B_\varphi = (H_\varphi + \sqrt{\gamma}\beta^r D^\theta)/\alpha$. This implies that $\Omega_{F,max}$, which is obtained for $D^2 \approx B^2$ at the horizon, depends on the structure of \mathbf{B}_p .

We have assumed that some field lines of \mathbf{B}_p produced by the external currents are threading the equatorial plane within the ergosphere in Sections 5.3 and 5.4 and in Fig. 5. However, a situation could be realized in which the magnetospheric currents around the equatorial plane become so strong that no field lines intersect the equatorial plane within the ergosphere, as demonstrated by some MHD numerical simulations (Komissarov 2005; Komissarov & McKinney 2007). The Blandford-Znajek process can operate only for the field lines threading the horizon in this case.

6.2 On the ideal MHD condition

The ideal MHD condition ($F_{\mu\nu}u^\nu = 0$) is $\hat{\mathbf{D}} + \hat{\mathbf{v}} \times \hat{\mathbf{B}} = 0$ as viewed by FIDOs. Beskin & Rafikov (2000) examined the two-fluid effects on the electron-positron plasma in the pulsar magnetosphere with a monopole magnetic field and the number density much larger than the Goldreich-Julian density, and showed that the one-fluid flow with the ideal MHD condition is a good approximation in the region $E^2 < B^2$ (see also Melatos & Melrose 1996; Goodwin et al. 2004). In this case, the ideal MHD condition does not imply the infinite isotropic conductivity, but rather, the flow is almost force-free and moving via the $\mathbf{E} \times \mathbf{B}$ drifts, i.e., $\mathbf{J}_p \parallel \mathbf{B}_p$. Most region in the BH magnetosphere may be described as the one-fluid with the ideal MHD condition or the force-free plasma in the same sense. However, this has to be violated in the current crossing region, as stated above. (The ideal MHD condition requires $D^2 < B^2$ from $|\hat{\mathbf{v}}| < 1$.)

For the pulsar case, the fluid at and inside the stellar surface has a high isotropic conductivity owing to the effective particle collisions, i.e., the particle collision rate is very high compared with the gyration period (cf. Bekenstein & Oron 1978; Khanna 1998), in which the poloidal currents flow across the poloidal magnetic field lines and the electromotive force arises. The ideal MHD condition is a good approximation there.

Beskin & Kusnetsova (2000) examined the one-fluid MHD flow in the Kerr BH magnetosphere with a small spin parameter $a \ll 1$ and a monopole magnetic field, and argued that there are many types of solutions corresponding to different values of H_φ and Ω_F (see their Table 1). The MHD flow in the Kerr BH magnetosphere generally consists of an inflow and an outflow, and they assumed that there is a gap between them, in which $\mathbf{D} \cdot \mathbf{B} \neq 0$ and the poloidal currents flow across the poloidal \mathbf{B} field lines. Some types of those solutions have a surface of $D^2 = B^2$ in the inflow, “inflow with shock” (see also Beskin et al. 1983; Beskin & Rafikov 2000), which appear to be consistent with our conclusion, while one of those solutions has no surfaces of $D^2 = B^2$ for which the ideal MHD condition is satisfied in the whole region except the gap region. Whether the latter type of the solution is realized depends on the nature of the gap and

possibly on the assumptions on a and the magnetic field structure, and this point remains to be further investigated.

6.3 Final remarks

The plasma may keep being injected into the whole Kerr BH magnetosphere through the electron-positron pair creation by collisions of two photons emitted from the external hot fluid and/or through electron-proton creation by decays of neutrons escaping from the external fluid (Toma & Takahara 2012). The electrons accelerated due to the strong \mathbf{D} field in the current crossing region produce photons, which also can create electron-positron pairs by collisions with the external photons. However, it will be hard for those electron-positron pairs to be distributed widely in the magnetosphere, because the poloidal drift motions ($\mathbf{D} \times \mathbf{B}_\varphi$) are downward in the region of $\Omega > \Omega_F$ (see Fig. 3).

The origin of the electromotive force in the Blandford-Znajek process is attributed to the ergosphere. It cannot work in the Schwarzschild BH magnetosphere, which has no ergosphere. Then it is expected that the rotational energy of the Kerr BH decreases by this process. However, it is not evident how the BH rotational energy is converted to the Poynting flux. This energy conversion mechanism has been discussed so far by utilizing the ideal MHD simulation results, focusing on the importance of generation of negative particle energies (Koide et al. 2002; Komissarov 2005). We have argued that the breakdown of the ideal MHD condition is essential for giving rise to the electromotive force. Further analyses on the energy transport are needed to fully understand the physics of the Blandford-Znajek process (see also Komissarov 2009).

ACKNOWLEDGMENTS

We thank the anonymous referee for his/her comments, which improved the manuscript. K.T. thanks Shinpei Shibata, Hideyuki Tagoshi, Yuto Teraki, and Shigeo Kimura for useful discussions. This work is partly supported by JSPS Research Fellowships for Young Scientists No.231446.

REFERENCES

Asano K., & Takahara F., 2009, ApJ, 690, L81
 Bardeen J.M., Press W.H., & Teukolsky S.A., 1972, ApJ, 178, 347
 Becker P.A., Das S., & Le T., 2011, ApJ, 743, 47
 Bejger M., Piran, T., Abramowicz M., & Hakanson F. 2012, Phys. Rev. Lett., 109, 121101
 Bekenstein J.D., & Oron E., 1978, PRD, 18, 1809
 Beskin V.S., 2010, Phys. Uspekhi, 53, 1199
 Beskin V.S., Gurevich A.V., & Istomin Y.N., 1983, Sov. Phys. JETP, 58, 235
 Beskin V.S., & Kusnetsova I.V., 2000, Nuovo Cimento B, 115, 795
 Beskin V.S., Istomin Y.N., & Pariev V.I., 1992, Sov. Astron., 36, 642
 Beskin V.S., & Rafikov R.R., 2000, MNRAS, 313, 433
 Blandford R.D., & Znajek R.L., 1977, MNRAS, 176, 465

Contopoulos I., Kazanas D., & Papadopoulos D.B., 2013, ApJ, 765, 113
 Goldreich P., Julian W.H., 1969, ApJ, 157, 869
 Goodwin S.P., Mestel J., Mestel L., & Wright G.A.E., 2004, MNRAS, 349, 213
 Hirotani K., & Okamoto I., 1998, ApJ, 497, 563
 Khanna, R., 1998, MNRAS, 294, 673
 King A.R., Lasota J.P., & Kundt W., 1975, Phys. Rev. D, 12, 3037
 Koide S., Shibata K., Kudoh T., & Meier D.L., 2002, Science, 295, 1688
 Komissarov S.S., 2004a, MNRAS, 350, 427
 Komissarov S.S., 2004b, MNRAS, 350, 1431
 Komissarov S.S., 2005, MNRAS, 359, 801
 Komissarov S.S., 2009, J. Korean Phys. Soc., 54, 2503
 Komissarov S.S., & Barkov M.V., 2009, MNRAS, 397, 1153
 Komissarov S.S., & McKinney J.C., 2007, MNRAS, 377, L49
 Landau L.D., & Lifshitz E.M., 1975, The Classical Theory of Fields, Course of Theoretical Physics, Vol. 2 (New York: Pergamon)
 Levinson A., 2006, in Trends in Black Hole Research, edited by Kreitler P.V. (Nova Science Publishers, New York), 119 (arXiv:astro-ph/0502346)
 Lovelace R.V.E., 1976, Nature, 262, 649
 McKinney J.C., 2006, MNRAS, 368, 1561
 Melatos A., & Melrose D.B., 1996, MNRAS, 279, 1168
 Menon G., & Dermer C.D., 2005, ApJ, 635, 1197
 Menon G., & Dermer C.D., 2011, MNRAS, 417, 1098
 Okamoto I., 2012, Publ. Astron. Soc. Japan, 64, 50
 Paczynski B., 1990, ApJ, 363, 218
 Penna R.F., Narayan R., & Sadowski A., MNRAS, 436, 3741
 Penrose R., 1969, Nuovo. Cim., 1, 252
 Punsly B., 2008, Black Hole Gravito-hydro-magnetics, 2nd Edition. Springer, Berlin
 Punsly B., & Coroniti F.V., 1989, Phys. Rev. D, 40, 3834
 Punsly B., & Coroniti F.V., 1990, ApJ, 354, 583
 Ruiz M., Palenzuela C., Galeazzi F., & Bona C., 2012, MNRAS, 423, 1300
 Takahashi M., Nitta S., Tatematsu Y., & Tomimatsu A., 1990, ApJ, 363, 206
 Tchekhovskoy, A., Narayan, R., & McKinney, J.C., 2011, MNRAS, 418, L79
 Thorne K.S., MacDonald D.A., 1982, MNRAS, 198, 339
 Thorne K.S., Price R.H., & MacDonald D.A., 1986, The Membrane Paradigm. Yale Univ. Press, New Haven, CT
 Toma K., & Takahara F., 2012, ApJ, 754, 148
 Toma K., & Takahara F., 2013, Prog. Theor. Exp. Phys., 2013, 083E02
 Wald R.M., 1974, Phys. Rev. D, 10, 1680

APPENDIX A: ELECTROMAGNETIC FIELD IN THE VACUUM

Wald (1974) showed a vacuum test electromagnetic field solution in Kerr space-time for which the magnetic field is uniform, parallel to the rotation axis, at infinity with the strength B_0 as

$$F_{\mu\nu} = B_0(\partial_{[\mu}\xi_{\nu]} + 2a\partial_{[\mu}\chi_{\nu]}), \quad (\text{A1})$$

where a is the dimensionless spin parameter. The covariant forms of the \mathbf{D} and \mathbf{B} fields are given by

$$D_\mu = F_{\mu\nu}n^\nu, \quad B^\mu = -{}^*F^{\mu\nu}n_\nu, \quad (\text{A2})$$

(Komissarov 2004a). In this sense, \mathbf{D} and \mathbf{B} are the electric and magnetic fields as measured by FIDOs. Here we calculate the strengths of the \mathbf{D} and \mathbf{B} fields of the vacuum solution in the BL and KS coordinates.

In the BL coordinates, one has the following non-zero metric components

$$\begin{aligned} \alpha &= \sqrt{\frac{\varrho^2 \Delta}{\Sigma}}, \quad \beta^\varphi = -\frac{2ar}{\Sigma}, \\ \gamma_{\varphi\varphi} &= \frac{\Sigma}{\varrho^2} \sin^2 \theta, \quad \gamma_{rr} = \frac{\varrho^2}{\Delta}, \quad \gamma_{\theta\theta} = \varrho^2, \end{aligned} \quad (\text{A3})$$

where

$$\begin{aligned} \varrho^2 &= r^2 + a^2 \cos^2 \theta, \quad \Delta = r^2 + a^2 - 2r, \\ \Sigma &= (r^2 + a^2)^2 - a^2 \Delta \sin^2 \theta, \end{aligned} \quad (\text{A4})$$

(see e.g. Landau & Lifshitz 1975). FIDOs can have a local orthonormal basis as

$$\begin{aligned} \omega^t &= \alpha dt, \quad \omega^\varphi = \sqrt{\gamma_{\varphi\varphi}}(\beta^\varphi dt + d\varphi), \\ \omega^r &= \sqrt{\gamma_{rr}} dr, \quad \omega^\theta = \sqrt{\gamma_{\theta\theta}} d\theta, \end{aligned} \quad (\text{A5})$$

which satisfy $ds^2 = \eta_{ab}\omega^a\omega^b$. The corresponding basis vectors are

$$\begin{aligned} e_t &= \frac{1}{\alpha}(\partial_t - \beta^\varphi \partial_\varphi), \quad e_\varphi = \frac{1}{\sqrt{\gamma_{\varphi\varphi}}}\partial_\varphi, \\ e_r &= \frac{1}{\sqrt{\gamma_{rr}}}\partial_r, \quad e_\theta = \frac{1}{\sqrt{\gamma_{\theta\theta}}}\partial_\theta. \end{aligned} \quad (\text{A6})$$

Note that $n^\mu = e_t^\mu$ and $n_\mu = -\omega_t^\mu$. Then we can calculate the vector components \hat{D}_i and \hat{B}^i in respect of the orthonormal basis as

$$\hat{D}_i = D_\mu e_i^\mu = F_{\mu\nu} e_i^\mu e_t^\nu, \quad \hat{B}^i = B^\mu \omega_\mu^i = \frac{1}{2} e^{\mu\nu\alpha\beta} F_{\alpha\beta} \omega_\mu^i \omega_\nu^t. \quad (\text{A7})$$

The result is

$$\begin{aligned} \hat{D}_\varphi &= \hat{B}^\varphi = 0, \\ \hat{D}_r &= \frac{B_0 a}{\sqrt{\Sigma} \rho^4} [2r^2 \rho^2 \sin^2 \theta - (r^2 + a^2)(r^2 - a^2 \cos^2 \theta)(1 + \cos^2 \theta)], \\ \hat{D}_\theta &= \frac{B_0 a^3 \sqrt{\Delta}}{\sqrt{\Sigma} \rho^4} 2r \sin \theta \cos \theta (1 + \cos^2 \theta), \\ \hat{B}^r &= \frac{B_0}{\sqrt{\Sigma} \rho^4} \cos \theta [(r^2 + a^2)(\rho^4 - 4ra^2 \cos^2 \theta) - 2ra^4 \sin^4 \theta], \\ \hat{B}^\theta &= \frac{-B_0 \sqrt{\Delta}}{\sqrt{\Sigma} \rho^4} \sin \theta [r\rho^4 + a^2(r^2 - a^2 \cos^2 \theta)(1 + \cos^2 \theta)]. \end{aligned} \quad (\text{A8})$$

This agrees with the result of the same calculation in King et al. (1975) and Punsly & Coroniti (1989). Because $D^\mu D_\mu$ and $B^\mu B_\mu$ are scalars and $\hat{D}^t = D^t = 0$ and $\hat{B}^t = B^t = 0$, one has $D^2 = \hat{D}^2$ and $B^2 = \hat{B}^2$. We calculate $\hat{D}^2/\hat{B}^2 = D^2/B^2$ and plot it in Figure 2.

In the KS coordinates, one has the following non-zero metric components

$$\begin{aligned} \alpha &= \frac{1}{\sqrt{1+z}}, \quad \beta^r = \frac{z}{1+z}, \quad \gamma_{\varphi\varphi} = \frac{\Sigma}{\rho^2} \sin^2 \theta, \\ \gamma_{r\varphi} &= -a(1+z) \sin^2 \theta, \quad \gamma_{rr} = 1+z, \quad \gamma_{\theta\theta} = \varrho^2 \end{aligned} \quad (\text{A9})$$

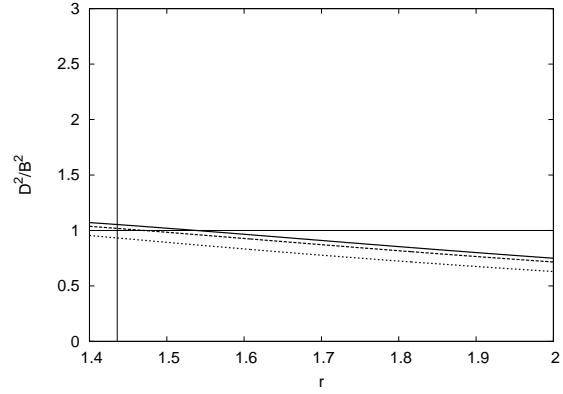


Figure A1. D^2/B^2 calculated for the Wald vacuum solution in the KS coordinates, as functions of r for $\theta = \pi/2$ (solid), 0.45π (dashed), and 0.4π (dotted). The spin parameter is set as $a = 0.9$. The vertical line represents the event horizon radius $r_H = 1.436$. The radius of the outer boundary of the ergosphere is $r_{\text{es}} = 2$ for $\theta = \pi/2$.

where $z = 2r/\varrho^2$ (Komissarov 2004a). By transferring the KS FIDO motion into the BL coordinates, one finds that the KS FIDO has the same angular velocity as the BL FIDO but also moves radially towards the true singularity. The orthonormal basis dual-vectors can be chosen as

$$\begin{aligned} \omega^t &= \alpha dt, \quad \omega^\varphi = \beta^r \frac{\gamma_{r\varphi}}{\sqrt{\gamma_{\varphi\varphi}}} dt + \sqrt{\gamma_{\varphi\varphi}} d\varphi + \frac{\gamma_{r\varphi}}{\sqrt{\gamma_{\varphi\varphi}}} dr, \\ \omega^r &= \sqrt{\frac{\gamma}{\gamma_{\varphi\varphi} \gamma_{\theta\theta}}} (\beta^r dt + dr), \quad \omega^\theta = \sqrt{\gamma_{\theta\theta}} d\theta, \end{aligned} \quad (\text{A10})$$

and the corresponding basis vectors are

$$\begin{aligned} e_t &= \frac{1}{\alpha} (\partial_t - \beta^r \partial_r), \quad e_\varphi = \frac{1}{\sqrt{\gamma_{\varphi\varphi}}} \partial_\varphi, \\ e_r &= \sqrt{\frac{\gamma_{\varphi\varphi} \gamma_{\theta\theta}}{\gamma}} \left(\partial_r - \frac{\gamma_{r\varphi}}{\gamma_{\varphi\varphi}} \partial_\varphi \right), \quad e_\theta = \frac{1}{\sqrt{\gamma_{\theta\theta}}} \partial_\theta, \end{aligned} \quad (\text{A11})$$

(Komissarov 2004b). Note that $n^\mu = e_t^\mu$ and $n_\mu = -\omega_t^\mu$, similar to those in the BL coordinates. Then by calculating equation (A7) we obtain

$$\begin{aligned} \hat{D}_\varphi &= \frac{B_0}{\sqrt{\Sigma} \rho^5 \sqrt{1+z}} 2r \sin \theta [r\rho^4 + a^2(r^2 - a^2 \cos^2 \theta)(1 + \cos^2 \theta)], \\ \hat{D}_r &= \frac{B_0 a}{\sqrt{\Sigma} \rho^4} [2r^2 \rho^2 \sin^2 \theta - (r^2 + a^2)(r^2 - a^2 \cos^2 \theta)(1 + \cos^2 \theta)], \\ \hat{D}_\theta &= \frac{B_0 a^3}{\rho^5 \sqrt{1+z}} 2r \sin \theta \cos \theta (1 + \cos^2 \theta), \\ \hat{B}^\varphi &= \frac{B_0 a^3}{\sqrt{\Sigma} \rho^5 \sqrt{1+z}} 4r^2 \sin \theta \cos \theta (1 + \cos^2 \theta), \\ \hat{B}^r &= \frac{B_0}{\sqrt{\Sigma} \rho^4} \cos \theta [(r^2 + a^2)(\rho^4 - 4ra^2 \cos^2 \theta) - 2ra^4 \sin^4 \theta], \\ \hat{B}^\theta &= \frac{-B_0}{\rho^5 \sqrt{1+z}} \sin \theta [r\rho^4 + a^2(r^2 - a^2 \cos^2 \theta)(1 + \cos^2 \theta)]. \end{aligned} \quad (\text{A12})$$

In Fig. A1 we plot $D^2/B^2 = \hat{D}^2/\hat{B}^2$ calculated in the KS coordinates. It does not show the divergence at the event horizon, unlike that calculated in the BL coordinates as

shown in Fig. 2. Note that the \mathbf{D} fields (as well as the \mathbf{B} fields) in the BL and KS coordinates are not identical, correspondingly to the difference of n^μ in equation (A2). Thus D^2 , B^2 , D^2/B^2 are different in the two coordinates, but $B^2 - D^2 = F_{\mu\nu}F^{\mu\nu}/2$ is a scalar, providing the same value in the two coordinates. This can be confirmed directly by using equations (A8) and (A12). As a result, the region of (r, θ) where $D^2/B^2 > 1$ (i.e., $D^2 - B^2 > 0$) are identical in Fig. 2 and Fig. A1.

APPENDIX B: PARTICLE MOTION AS VIEWED BY FIDOS

The equation of a particle motion as viewed by FIDOS is described as

$$\frac{D\hat{u}_\mu}{d\tau} = \frac{q}{m} \hat{F}_{\mu\nu} \hat{u}^\nu, \quad (\text{B1})$$

where τ , q , and m are the proper time, charge, and mass of a particle, respectively. For $\mu = \varphi$ in the BL coordinates as an example, one has

$$\begin{aligned} \hat{F}_{\varphi t} &= F_{\alpha\beta} e_\varphi^\alpha e_t^\beta = \hat{D}_\varphi, \\ \hat{F}_{\varphi r} &= F_{\alpha\beta} e_\varphi^\alpha e_r^\beta \\ &= e_{\varphi r \theta} B^\theta \frac{1}{\sqrt{\gamma_{\varphi\varphi}}} \frac{1}{\sqrt{\gamma_{rr}}} = \sqrt{\gamma_{\theta\theta}} B^\theta = \hat{B}^\theta, \\ \hat{F}_{\varphi \theta} &= F_{\alpha\beta} e_\varphi^\alpha e_\theta^\beta \\ &= e_{\varphi \theta r} B^r \frac{1}{\sqrt{\gamma_{\varphi\varphi}}} \frac{1}{\sqrt{\gamma_{\theta\theta}}} = -\sqrt{\gamma_{rr}} B^r = -\hat{B}^r, \end{aligned}$$

where we have used $F_{ij} = e_{ijk} B^k$ (see Komissarov 2004a). Thus one obtains

$$\frac{D\hat{u}_\varphi}{d\tau} = \frac{q}{m} (\hat{D}_\varphi \hat{u}^t + \epsilon_{\varphi jk} \hat{u}^j \hat{B}^k). \quad (\text{B2})$$

The same form of equation is obtained also for $\mu = r$ and θ . By taking account of $d\tau = dt/\hat{u}^t$ and the assumption that the gravitational force is negligible compared with the Lorentz force, one obtains equation (27). The same form of the equation is obtained also by using the KS coordinates.

Let us examine the drift motion of a particle in the plasma with $\mathbf{D} \cdot \mathbf{B} = 0$ in the BL coordinates. From equation (29), one has $D_r = (\sqrt{\gamma}/\alpha)(\Omega_F - \Omega)B^\theta$, $D_\theta = (-\sqrt{\gamma}/\alpha)(\Omega_F - \Omega)B^\theta$, and $D_\varphi = 0$. The drift three-velocity as viewed by FIDOS is $\hat{v}_d = (\hat{\mathbf{D}} \times \hat{\mathbf{B}})/\hat{B}^2$, where $\hat{B}^2 = B^2$. The azimuthal drift velocity is calculated as

$$\hat{v}_d^\varphi = \frac{D_r B_\theta - D_\theta B_r}{B^2 \sqrt{\gamma_{rr} \gamma_{\theta\theta}}} = \frac{\sqrt{\gamma_{\varphi\varphi}}}{\alpha} (\Omega_F - \Omega) \frac{B_p^2}{B^2}. \quad (\text{B3})$$

In general, one has $\hat{u}^t = u^\mu \omega_\mu^t = \alpha u^t$ and $\hat{u}^\varphi = u^\mu \omega_\mu^\varphi = \sqrt{\gamma_{\varphi\varphi}}(u^\varphi - \Omega u^t)$. Then $\hat{v}^\varphi = \hat{u}^\varphi/\hat{u}^t = (\sqrt{\gamma_{\varphi\varphi}}/\alpha)(v^\varphi - \Omega)$. Therefore, one finds

$$v_d^\varphi = \Omega_F \left(1 - \frac{B_\varphi B^\varphi}{B^2}\right) + \Omega \frac{B_\varphi B^\varphi}{B^2}. \quad (\text{B4})$$

When $\hat{B}_\varphi = B_\varphi = 0$, one has $v_d^\varphi = \Omega_F$. In this case, $\hat{v}_d^\varphi = \pm 1$ at the light surfaces, where $\Omega_F - \Omega = \pm \alpha/\sqrt{\gamma_{\varphi\varphi}}$.

When $B_\varphi \neq 0$, one has non-zero poloidal components of the drift velocity,

$$\hat{v}_d^r = \frac{D_\theta B_\varphi}{B^2 \sqrt{\gamma_{\theta\theta} \gamma_{\varphi\varphi}}}, \quad \hat{v}_d^\theta = \frac{-D_r B_\varphi}{B^2 \sqrt{\gamma_{rr} \gamma_{\varphi\varphi}}}. \quad (\text{B5})$$

Then one has $v_d^r = \hat{v}_d^r/\sqrt{\gamma_{rr}} = (\mathbf{D} \times \mathbf{B}_\varphi)^r/B^2$ and $v_d^\theta = \hat{v}_d^\theta/\sqrt{\gamma_{\theta\theta}} = (\mathbf{D} \times \mathbf{B}_\varphi)^\theta/B^2$. This means that

$$\mathbf{v}_d^p \parallel (\mathbf{D} \times \mathbf{B}_\varphi). \quad (\text{B6})$$

APPENDIX C: CHARGE DENSITY DISTRIBUTION

We derive a description of the charge distribution which is valid for $f(\Omega_F, r, \theta) < 0$ in the case of $\mathbf{D} \cdot \mathbf{B} = 0$ and $B_\varphi = 0$ in the BL coordinates. By using equations (29) and (18), one has

$$\begin{aligned} 4\pi\rho &= \nabla \cdot \mathbf{D} = \nabla \cdot \left[\frac{-1}{\alpha} (\boldsymbol{\omega} + \boldsymbol{\beta}) \times \mathbf{B} \right] \\ &= \frac{\gamma_{\varphi\varphi}(\Omega_F - \Omega)}{\alpha^2 \sqrt{\gamma}} (\partial_r H_\theta - \partial_\theta H_r) \\ &\quad + \frac{1}{\sqrt{\gamma}} (H_\theta \partial_r - H_r \partial_\theta) \frac{\gamma_{\varphi\varphi}(\Omega_F - \Omega)}{\alpha^2} \\ &\quad - \frac{\gamma_{\varphi\varphi}(\Omega_F - \Omega)\Omega}{\alpha^2} \nabla \cdot \mathbf{D} \\ &\quad - \mathbf{D} \cdot \nabla \left[\frac{\gamma_{\varphi\varphi}(\Omega_F - \Omega)\Omega}{\alpha^2} \right]. \end{aligned} \quad (\text{C1})$$

The particle drift motions carry the current as measured by FIDOS, $\hat{j}^\varphi = \rho \hat{v}_d^\varphi$, which is equivalent to $j^\varphi = (\rho/\alpha)(v_d^\varphi - \Omega)$. By using $J^\varphi = \alpha j^\varphi + \rho\Omega$ (Equation 19), one has

$$\partial_r H_\theta - \partial_\theta H_r = 4\pi\sqrt{\gamma} J^\varphi = 4\pi\sqrt{\gamma}\rho\Omega_F. \quad (\text{C2})$$

Then one obtains (by using equation 18 again)

$$\begin{aligned} \rho &= \frac{\alpha^2}{4\pi f(\Omega_F, r, \theta)} \left[\frac{\gamma_{\varphi\varphi}(\Omega_F - \Omega)}{\alpha^2} (D^r \partial_r + D^\theta \partial_\theta)\Omega \right. \\ &\quad \left. - \frac{\alpha}{\sqrt{\gamma}} (B_\theta \partial_r - B_r \partial_\theta) \frac{\gamma_{\varphi\varphi}(\Omega_F - \Omega)}{\alpha^2} \right] \end{aligned} \quad (\text{C3})$$

This equation can be reduced to

$$\begin{aligned} \rho &= \frac{\alpha^2}{4\pi f(\Omega_F, r, \theta)} \left\{ \frac{\gamma_{\varphi\varphi}}{\alpha\sqrt{\gamma}} \left[\frac{\gamma_{\varphi\varphi}(\Omega_F - \Omega)^2}{\alpha^2} + 1 \right] (B_\theta \partial_r - B_r \partial_\theta)\Omega \right. \\ &\quad \left. - \frac{\alpha}{\sqrt{\gamma}} (\Omega_F - \Omega) (B_\theta \partial_r - B_r \partial_\theta) \frac{\gamma_{\varphi\varphi}}{\alpha^2} - \frac{\gamma_{\varphi\varphi}}{\alpha} B_p^2 \frac{d\Omega_F}{d\Psi} \right\} \end{aligned} \quad (\text{C4})$$

The charge density ρ can be calculated if \mathbf{B}_p and $\Omega_F(\Psi)$ are given.

Let us calculate ρ by assuming \mathbf{B}_p as the Wald vacuum solution (equation A8). This corresponds to the Goldreich-Julian charge density for the Kerr BH magnetosphere. For $\Omega_F = \Omega_H/2$, we confirmed that our calculation result of the surface of $\rho = 0$ is consistent with Fig. 3 of Beskin et al. (1992). For $\Omega_F = 0$, we obtain the result as shown in Figure C1.

For the case of non-uniform Ω_F , the flux function Ψ is required to calculate ρ . For the Wald solution of the \mathbf{B} field, it is given as (Beskin et al. 1992)

$$\Psi = \frac{B_0 \sin^2 \theta}{2a^2} (\Sigma - 4a^2 r). \quad (\text{C5})$$

It is confirmed that this form of Ψ provides the \mathbf{B} field in equation (A8) through equation (22).

As an example, we assume the Wald solution of the \mathbf{B}_p field and Ω_F given as

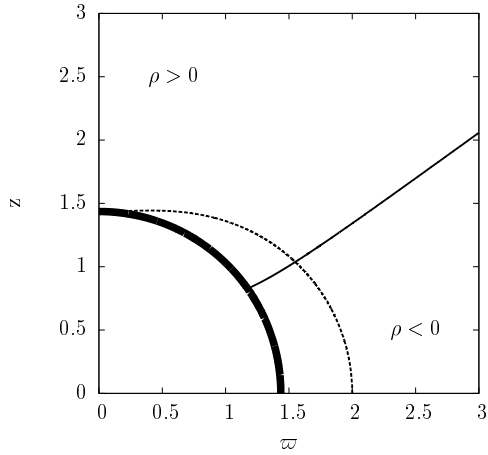


Figure C1. Charge density distribution for the Wald \mathbf{B}_p field with $\mathbf{D} \cdot \mathbf{B} = 0$ and $\Omega_F = 0$. The surface of $\rho = 0$ is represented by the thin black line. One has $\rho < 0$ under this line and outside the event horizon (the thick black line). The inner light surface is identical to the outer boundary of the ergosphere (the dashed line).

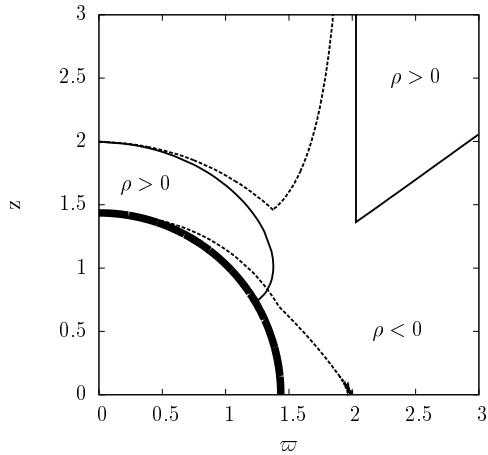


Figure C2. Charge density distribution for the Wald \mathbf{B}_p field with $\mathbf{D} \cdot \mathbf{B} = 0$ and Ω_F given by equation (C6). The surface of $\rho = 0$ is represented by the solid lines. In the region surrounded by the two solid lines and the event horizon (the thick solid line), one has $\rho < 0$. The inner dashed line represents the inner light surface, and the outer dashed line the surface of $\Omega = \Omega_F$.

$$\Omega_F(\Psi) = \begin{cases} \Omega_H/2 & \text{for } \varpi_{\text{eq}}(\Psi) \leq r_H \\ \frac{\Omega_H}{2} \frac{r_{\text{es}} - \varpi_{\text{eq}}(\Psi)}{r_{\text{es}} - r_H} & \text{for } r_H < \varpi_{\text{eq}}(\Psi) < r_{\text{es}} \\ 0 & \text{for } \varpi_{\text{eq}}(\Psi) \geq r_{\text{es}}, \end{cases} \quad (\text{C6})$$

where $\varpi_{\text{eq}}(\Psi)$ is the cylindrical radius at which a \mathbf{B} field line crosses the equatorial plane. This form satisfies $\Omega_F \lesssim \Omega_{F,\text{max}}$ for the \mathbf{B} field lines threading the equatorial plane outside the event horizon, where $\Omega_{F,\text{max}}$ is given by equation (33) (see also Fig. 4). The calculation result is shown in Fig. C2.

This paper has been typeset from a $\text{T}_{\text{E}}\text{X}/\text{L}^{\text{A}}\text{T}_{\text{E}}\text{X}$ file prepared by the author.